FINITE ELEMENT ANALYSIS FOR THE STRUCTURAL BEHAVIOUR OF PAVING FLAGS MADE BY OC AND UHPFRC

Dr. **LE TRUNG THANH**
Vietnam Institute for Building Materials (VIBM)

Abstract: *Ultra High Performance Fibre Reinforced Concrete (UHFRPC) having over 150 MPa compressive strength and 15-40 MPa flexural strength is considered as the latest generation of concrete technology and highly advanced performance compared with other high strength concretes. UHPFRC is therefore effective in use for the structural components carrying flexural loads such as paving flags.*

This paper presents the research outcome based on finite element analysis modelling of paving flags made by UHPFRC compared with ordinary concrete (OC). A model was created using finite element analysis (FEA) package, it comprises subbase, sand bedding, paving flag and loading plate. Loads were applied at various values to investigate the structural behaviour of paving flags, sand bedding and subbase layers. The modelling results agreed well with the experimental results.

Keywords: *UHPFRC, paving flag, FEA, stress, strain, failure load, displacement.*

Tóm tắt: *Bê tông cốt sợi tính năng siêu cao (UHPFRC) với cường độ chịu nén hơn 150 MPa và cường độ chịu uốn khoảng 15 - 40 MPa là đại diện cho thế hệ mới nhất của công nghệ bê tông, có tính năng siêu việt so với các loại bê tông cường độ cao khác. Vì vậy, UHPFRC rất hiệu quả khi sử dụng chế tạo các kết cấu chịu lực uốn như các tấm lát vỉa hè.*

Bài báo này trình bày các kết quả nghiên cứu dựa trên việc mô phỏng phân tích phần tử hữu hạn của các tấm lát vỉa hè làm bằng UHPFRC và so sánh với các tấm lát vỉa hè làm bằng bê tông thường (OC). Một mô hình kết cấu đã được tạo ra sử dụng phương pháp phân tích phần tử hữu hạn, nó bao gồm các lớp kết cấu móng đường, lớp cát đệm, tấm lát và tấm kê gia tải. Mô hình này được gia tải với các giá trị tải trọng khác nhau để nghiên cứu ứng xử kết cấu của các tấm lát, lớp cát đệm và lớp kết cấu móng đường. Các kết quả thu được từ mô phỏng kết cấu và các kết quả đo được từ thử nghiệm thực tế có độ tương đồng với nhau.

Từ khóa: *UHPFRC, tấm lát vỉa hè, phân tích phần tử hữu hạn FEA, ứng suất, biến dạng, tải trọng phá hủy, chuyển vị.*

1. Introduction

Finite element analysis (FEA) method was first introduced in the 1950s and has been continually developed and improved since then [1, 2]. However, computer modelling appears not to have been used extensively for concrete flag pavements. The most notable work was done by Bull and Al-Khalid [3, 4] who modelled an experimental set-up of a single ordinary concrete paving flag positioned on support layers such as sand bedding, sub-base and soil (subgrade). Bull and Khalid investigated only square paving flags as they are structurally more efficient than rectangular flags. Eight node rectangular brick elements were used to model the paving flag as well as the pavement layers. A total of 800 finite elements were used to model the pavement. The research tried to approach a pavement structure design. The thickness and California bearing ratio (CBR) of the sub-base and subgrade layers were investigated to let paving flags behave as an acceptable paving material, i.e. the maximum tensile concrete stress due to vehicular loading must be less than the manufacturing design load (4.8 MPa). It is generally accepted that the smaller the plan area of the flag the better it will perform. It is also generally accepted that the thickness of the flag is the main factor influencing the load capacity of a pavement. The research [3, 4] showed that the majority of the 50 mm thick ordinary concrete flags would crack for a standard axle load of 80 kN. Increasing the paving flag thickness may appear to be a way to increase its load bearing capacity, but this may not be desirable as problems will arise in handling especially if the weight exceeds 25 kg. However, this study investigated the structural behaviour of a paving flag working in the elastic region. This means that the insight into failure load

and cracking region of pavement under load, which are believed to be very important in structural design, has not been clarified.

The ways of predicting the structural behaviour of concrete ground-supported slabs can be referred for paving flags. The FEA studies of concrete ground-supported slabs usually model a slab positioned on a sub-base. Loading positions are popularly placed at the centre, edge and corner of slab [5-7], see an example shown in figure 1. Those studies tried to predict the failure load of concrete slabs and to compare with the experimental failure load. A study carried out by Falkner et al [7] simulated some 3 x 3 x 0.15 m slabs using Steel fibre reinforced concrete (SFRC) and plain concrete

for comparison. They named the slab using plain concrete as P1 while the slabs using SFRC with 30 kg mill cut steel fibres per m^3 concrete and 20 kg hooked end steel fibres per m^3 of concrete were named as P2 and P3. Concrete grade C35 (fcu = 35 MPa) was used for the slabs. A 12 x 12 cm loading plate was placed in the centre of slabs. Their result is shown in figure 2. The authors claimed that the failure loads predicted by FEA modelling of slabs showed a good agreement with the experimental results. The conclusions also stated that slabs using SFRC were able to redistribute the stresses until the plastic hinges occurred at the main cracks and they could still maintain their slab action while the slab using plain concrete failed at early stage.
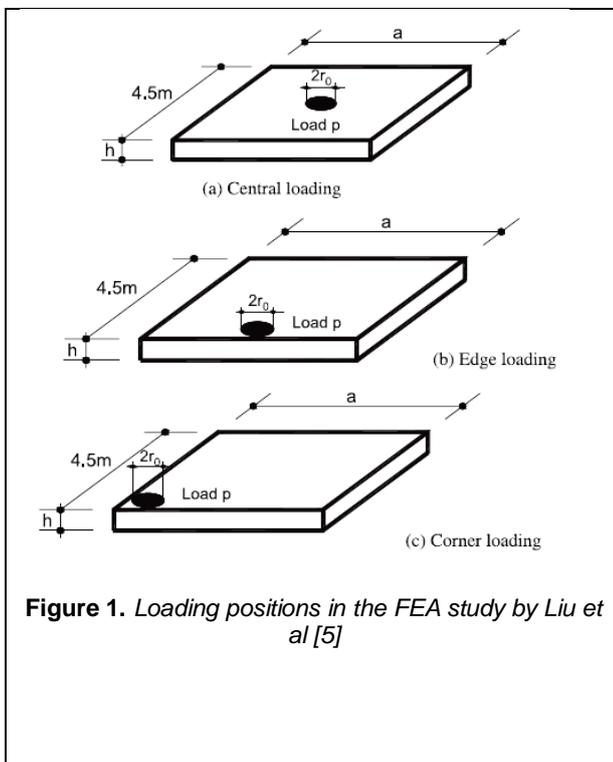

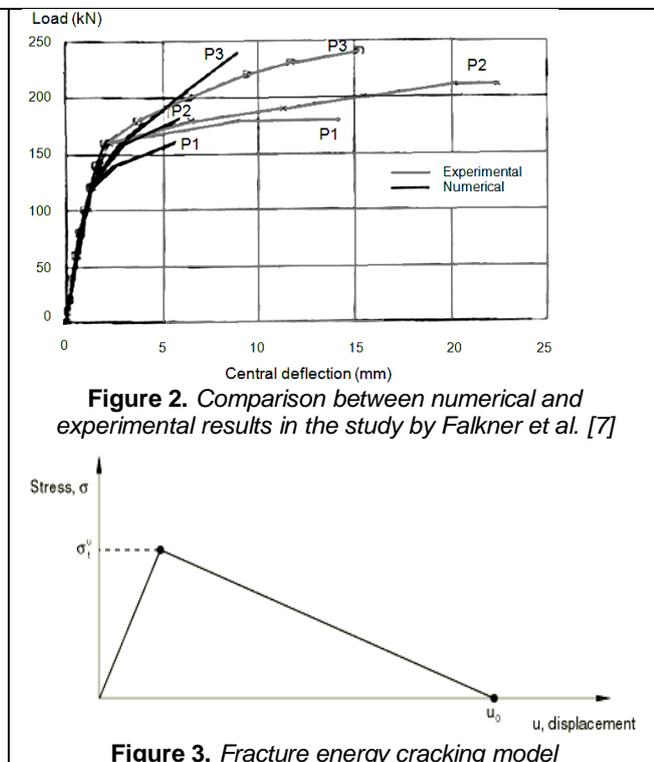**Figure 1.** *Loading positions in the FEA study by Liu et al [5]*

Figure 2. *Comparison between numerical and experimental results in the study by Falkner et al. [7]*

Figure 3. *Fracture energy cracking model*

The FEA studies [5-7] of concrete ground-supported slabs suggested that the material modelling reinforced concrete or fibre reinforced concrete should present a ductile failure in flexure but the material modelling plain concrete should present a brittle failure.

One of FEA software packages which has been recently used to analyse the behaviour of concrete ground-supported slab pavements [6, 8, 9] is ABAQUS. A number of recent FEA studies on UHPFRC bridge beams [10] and monorail girders

[11] have also used ABAQUS as a powerful tool to predict the failure loads. In the modelling cases involving static loads ABAQUS/Standard version is usually used. This FEA software offers the "concrete smeared cracking" material model which is suitable for both plain concrete and reinforced concrete [12]. This material model has been developed based on Hillerborg et al's concrete cracking model. Hillerborg et al defines the energy required to open a unit area of crack as a material parameter and calls it fracture energy (G_f) [13]. With this approach the concrete's behaviour is characterised by a stress-displacement

response rather than a stress-strain response. The fracture energy cracking model used for "concrete smeared cracking" material is shown in figure 3.

The fracture energy (G_f) is measured by the area under the tensile stress-displacement ($\sigma_t^u - u_0$) curve. The ultimate displacement, u_0, can be estimated from the fracture energy per unit area, G_f, as $u_0 = 2G_f/\sigma_t^u$, where σ_t^u is the maximum tensile stress that the concrete can carry. According to ABAQUS/Standard Manual [12], the typical value of u_0 is 0.05 mm for a normal concrete, i.e. brittle fracture. For reinforced concrete and fibre reinforced concrete, this value, u_0, depends on the magnitude of fracture energy in the ductile post-cracking mode. "Concrete smeared cracking" material model also has been used in a number of recent studies on UHPFRC bridge beams [10] and monorail girders [11]. Therefore, ABAQUS/Standard is used as the tool to model the pavements with two different types of concrete paving flags, i.e. normal concrete and UHPFRC, in this research.

To carry out a modelling process in the ABAQUS software package, the following nine modules need to be used:

1. Part: This module is to create each part in the model which needs to be analysed;

2. Property: This module is to define and assign materials for the parts of the model;

3. Assembly: This module defines the geometry of the finished model by creating instances of a part, i.e. the user can create instances of each part with the same properties and dimensions, and then positioning the instances relative to each other in a global coordinate system;

4. Step: This module is used to define the analysis steps and also to request output for any steps in the analysis;

5. Interaction: This module is used to define the contact interactions between part instances;

6. Load: This module is used to define the loads and boundary conditions applied to the model;

7. Mesh: This module is used to define the element types and generate meshes for the model;

8. Job: This module is used to create and submit an analysis job for processing;

9. Viewing the output from analysis: The output of analysis can be viewed either using the visualization module or the data file. The visualisation module enables a display and animation of the undeformed/deformed shape or contour plot while the data file gives detailed results as requested in the Step module.

This research presents the procedure for using the FEA method, i.e. ABAQUS/Standard package, to simulate a section of pavement with a single flag loaded with a square loading plate. The modelling results of the structural behaviour such as the compressive stress of sub-base layer; the displacement, tensile strain, failure load and cracking position of the paving flag are shown and compared to the experimental results. The use of FEA modelling attempted to clarify the insight into the structural behaviour of the paving flag carrying a square load plate.

2. FEA modelling

A FEA model was created to simulate a section of a pavement that comprised a 250 mm thick sub-base layer, a 40 mm thick sand bedding layer and a single paving flag positioned at the centre of the sand bedding layer and tested with a 100 mm square loading plate. The experimental arrangement had two strain gauges (S1 and S2) attached at the central underside of the paving flag and four displacement transducers (D1 to D4) set up on the upper surface of the paving flag, see Figure 4. The compressive stress at the central bottom of sub-base layer was measured using two stress gauges. All stresses, strains and displacements were recorded using a data acquisition system and the values were used to compared with the results obtained from the FEA model.
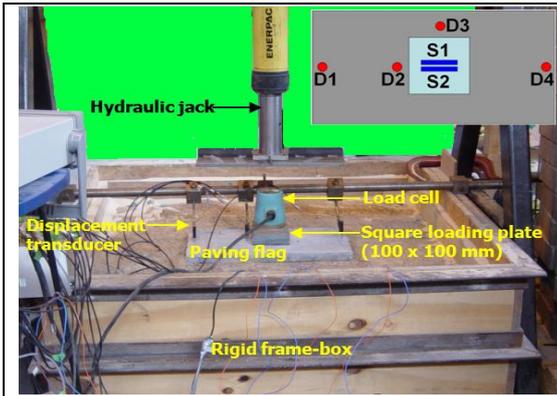
Figure 4. *Experimental arrangement of a single paving flag showing the positions of displacement transducers (D1 to D4) and strain gauges (S1 and S2)*
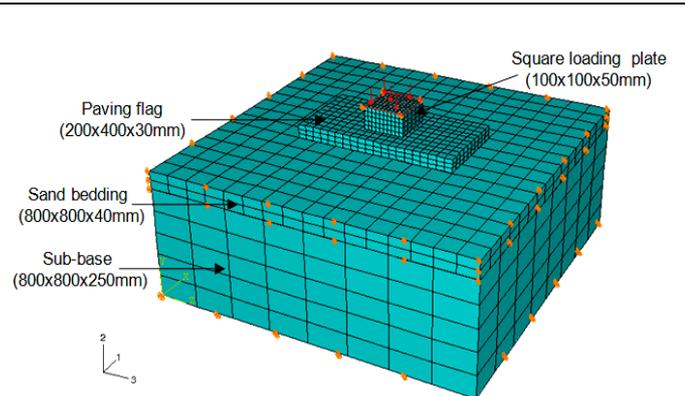

Figure 5. *Single paving flag loaded centrally - FEA model in ABAQUS/Standard*

The model comprised a 800x800x250 mm sub-base layer, a 800x800x40 mm sand bedding layer, a 400x200x30 mm paving flag and a 100x100x50mm loading plate. They were then assembled, as shown in Figure 5, using a "surface-to-surface" standard contact between each other. The details of critical steps in creating the model are as follows.

- Materials used for the model

Elastic materials were assigned for sub-base, sand bedding and loading plate while "concrete smeared cracking" material was assigned for a paving flag.

An elastic material model is valid for small elastic strains (normally less than 5%) and can be isotropic, orthotropic, or fully anisotropic [12]. The total stress is defined from the total elastic strain as shown in equation 1. Elastic materials are defined in ABAQUS/Standard by using elastic modulus and Poisson's ratio, see table 1.

$$\sigma = E.\varepsilon \qquad \text{(Equation 1)}$$

where: σ is the total stress;

E is the elastic modulus;

ε is the total elastic strain.

The smeared crack concrete model, an inelastic constitutive model [12, 14-16] using concepts of oriented damaged elasticity (smeared cracking) and isotropic compressive plasticity are to represent the inelastic behaviour of concrete. In concrete smeared cracking model, the stress-strain relation [14] is shown in equation 2.

$$
\begin{bmatrix} \Delta\sigma_{11} \\ \Delta\sigma_{22} \\ \Delta\sigma_{33} \\ \Delta\sigma_{12} \\ \Delta\sigma_{23} \\ \Delta\sigma_{31} \end{bmatrix} =
\begin{bmatrix}
\frac{\partial\sigma_{11}}{\partial\varepsilon_{11}} & \frac{\partial\sigma_{11}}{\partial\varepsilon_{22}} & \frac{\partial\sigma_{11}}{\partial\varepsilon_{33}} & 0 & 0 & 0 \\
\frac{\partial\sigma_{22}}{\partial\varepsilon_{11}} & \frac{\partial\sigma_{22}}{\partial\varepsilon_{22}} & \frac{\partial\sigma_{22}}{\partial\varepsilon_{33}} & 0 & 0 & 0 \\
\frac{\partial\sigma_{33}}{\partial\varepsilon_{33}} & \frac{\partial\sigma_{33}}{\partial\varepsilon_{22}} & \frac{\partial\sigma_{33}}{\partial\varepsilon_{33}} & 0 & 0 & 0 \\
0 & 0 & 0 & \frac{\sigma_{11}-\sigma_{22}}{2(\varepsilon_{11}-\varepsilon_{22})} & 0 & 0 \\
0 & 0 & 0 & 0 & \frac{\sigma_{22}-\sigma_{33}}{2(\varepsilon_{22}-\varepsilon_{33})} & 0 \\
0 & 0 & 0 & 0 & 0 & \frac{\sigma_{33}-\sigma_{11}}{2(\varepsilon_{33}-\varepsilon_{11})}
\end{bmatrix}
\begin{bmatrix} \Delta\varepsilon_{11} \\ \Delta\varepsilon_{22} \\ \Delta\varepsilon_{33} \\ \Delta\gamma_{12} \\ \Delta\gamma_{23} \\ \Delta\gamma_{31} \end{bmatrix}
$$

(Equation 2)

where: $\sigma_{11}, \sigma_{22}, \sigma_{33}$ are principal stresses;

$\sigma_{12}, \sigma_{23}, \sigma_{31}$ are shear stresses;

$\varepsilon_{11}, \varepsilon_{22}, \varepsilon_{33}$ are principal strains;

$\gamma_{12}, \gamma_{23}, \gamma_{31}$ are shear strains.

The total strain $\Delta\varepsilon$ of the cracked concrete is decomposed into a part $\Delta\varepsilon^{cr}$ of the crack and a part $\Delta\varepsilon^{co}$ of the solid as shown in equation 3.

$$\Delta\varepsilon = \Delta\varepsilon^{cr} + \Delta\varepsilon^{co} \qquad \text{(Equation 3)}$$

The importance of the decomposition is an attempt to come closer to the discrete crack concept which completely separates the solid material from the crack by using separate finite elements.

The model is defined by using elastic properties (elastic modulus and Poisson's ratio) and inelastic properties (compressive strength, plastic strain, failure tensile stress and ultimate displacement), see table 1. The failure tensile stress and ultimate displacement defines the fracture energy of concrete.

Cracking dominates the material behaviour when the state of stress is predominantly tensile. The model uses a "crack detection" plasticity surface in stress space to determine when cracking takes place, i.e. failure in tension. Damaged elasticity is then used to describe the post failure behaviour of the concrete with open cracks [17]. Numerically the "crack detection" plasticity model is used for the increment in which cracking takes place and subsequently damaged elasticity is used once

the crack's presence and orientation have been detected. As a result there is at least one increment in which we calculate crack detection "plastic" strains. As the fracture energy concept is used, the strains are related to the stress/displacement definition for the tension stiffening behaviour [17] by equation 4.

$$\Delta\varepsilon = \frac{u}{c} \qquad \text{(Equation 4)}$$

where: u is ultimate displacement;

c is the characteristic length associated with the integration point.

The difference between ordinary concrete flag and UHPFRC flag was determined by the input parameter of fracture energy (based on failure tensile stress and ultimate displacement). The material properties used for the model are shown in table 1. The fracture energy is defined as the area under the tensile stress - displacement curve of concrete, shown in figure 6.
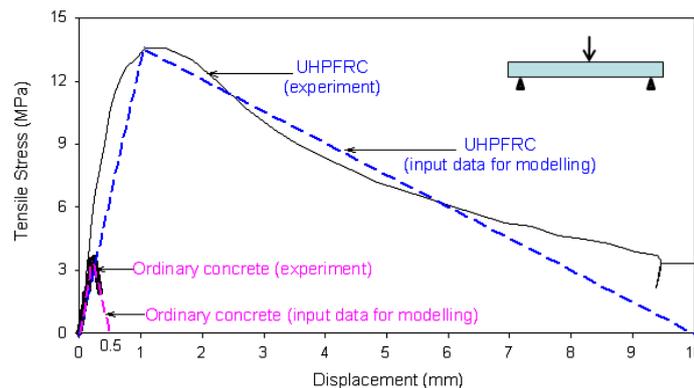
Figure 6. *Tensile stress versus displacement relationships used as the fracture energy inputs for ordinary concrete and UHPFRC flags*

Table 1. *Material properties used for finite element modelling*

Part (dimension, mm)	Properties						
	Density (kg/m³)	Elastic modulus (MPa)	Poisson ratio	Compressive strength (MPa)	Plastic strain	Failure tensile stress (MPa)	Ultimate Displacement (mm)
Sub-base (800x800x250 mm)	2,000*	200	0.25*	N/A	N/A	N/A	N/A
Sand bedding (800x800x40 mm)	1,800*	50*	0.25*	N/A	N/A	N/A	N/A
Square loading plate	7,850*	210,000*	0.3*	N/A	N/A	N/A	N/A
Ordinary concrete flag (200x400x30 mm)	2,400	29,000*	0.15*	45	0*	3.6	0.5
				0*	0.002*		
UHPFRC flag (200x400x30 mm)	2,500	55,000*	0.2*	150*	0*	13.6	10.0
				170	0.002*		
				120*	0.004*		
				50*	0.005*		

* Data are assumed by referring the references [3, 12, 18, 19]

The maximum tensile stresses were converted from the flexural stresses measured for the paving flags (three-point bending test). The values of maximum tensile stresses were also referred carefully to the ratios of tensile strength – compressive strength recommended by the ABAQUS manual for "concrete smeared cracking model" [12] and the ratios recommended in the manual book of numerical methods in concrete authored by Bangash [20]. Consequently, the ratios of maximum tensile stress-flexural strength and the ratios of maximum tensile stress-compressive strength used in this FEA modelling were as follows:

- For ordinary concrete paving flag:

$$\frac{\text{maximum tensile stress } (\sigma_t^u)}{\text{compressive strength } (\sigma_c)} = \frac{3.6}{45} = 0.08 \quad \text{(Equation 5)}$$

$$\frac{\text{maximum tensile stress } (\sigma_t^u)}{\text{flexural strength } (\sigma_b)} = \frac{3.6}{6} = 0.6 \quad \text{(Equation 6)}$$

- For UHPFRC paving flag:

$$\frac{\text{maximum tensile stress } (\sigma_t^u)}{\text{compressive strength } (\sigma_c)} = \frac{13.6}{170} = 0.08 \quad \text{(Equation 7)}$$

$$\frac{\text{maximum tensile stress } (\sigma_t^u)}{\text{flexural strength } (\sigma_b)} = \frac{13.6}{20} = 0.68 \quad \text{(Equation 8)}$$

The input value for the ultimate displacement of ordinary concrete was very small, i.e. 0.5 mm, modelling a brittle failure, while that of UHPFRC was 10.0 mm, modelling a ductile material. Although the tensile stress versus displacement model for UHPFRC used in ABAQUS might not match perfectly with the experimental behaviour, the most important criteria, i.e. failure tensile stress and approximate fracture energy, were an acceptable fit.

- Interactions

The interactions between the parts of the model were assigned as "surface-to-surface" standard with contact property as "hard contact" normal behaviour. This is a surface constitutive model. The definition of "hard contact" between two surfaces at a point, p, as a function of the "overclosure", h, of the surfaces (the interpenetration of the surfaces) is as follows [12].

p = 0   for h < 0 (open), and

h = 0   for p < 0 (closed)   (Equation 9)

A small-sliding property was also used in modelling the interactions between parts (deformable bodies) in three dimensions. With this approach, one surface definition provides "master" surface and the other surface definition provides the "slave" surface.

- Boundary conditions

In the FEA software ABAQUS, there are two coordinate systems that are the global coordinate system (X,Y,Z) and the local coordinate system (1,2,3). To replicate the boundary conditions of the experiment, the bottom of the sub-base layer was fixed in all three directions while the sides of the sub-base layer and sand bedding layer were only fixed in two horizontal directions that were X axis and Z axis (or 1 axis and 3 axis respectively), i.e. they still moved in Y vertical direction or 2 axis. The paving flag was not fixed in any directions.

- Applying load

Load was applied on the central square plate as a pressure, i.e. the unit used was N/mm^2, in small increments to find out the failure load of paving flags.

For the ordinary concrete flag pavement, the load was applied in the increment of 0 – 2 – 3 – 4 – 5 – 6 – 10 kN, i.e. 0 – 0.2 – 0.3 – 0.4 – 0.5 – 0.6 – 1.0 N/mm^2.

For the UHPFRC flag pavement, the load was applied in the increment of 0 – 5 – 10 – 12 – 14 – 15 – 18 – 21 – 24 – 34 kN, i.e. 0 – 0.5 – 1.0 – 1.2 – 1.5 – 1.8 – 2.1 – 2.4 – 3.4 N/mm^2.

- Meshing the model

Linear 8-node brick elements were used for all parts of the model. The size and number of elements used to simulate this pavement are shown in table 2. The model comprised 3,002 nodes and 1932 elements after being meshed.

The modelling results obtained were compared with the experimental results to approach an explanation of the failure mechanism of paving flag. This model also set up the essential reliance to carry out modelling of full pavement.

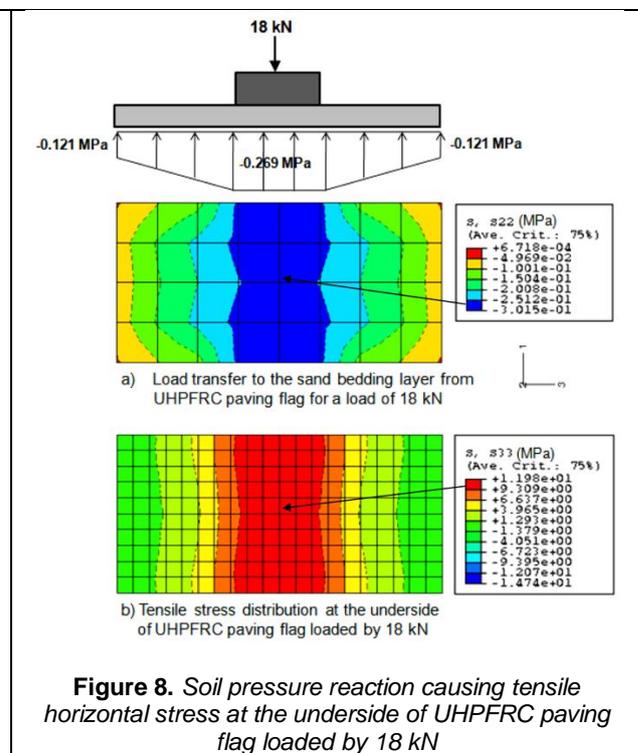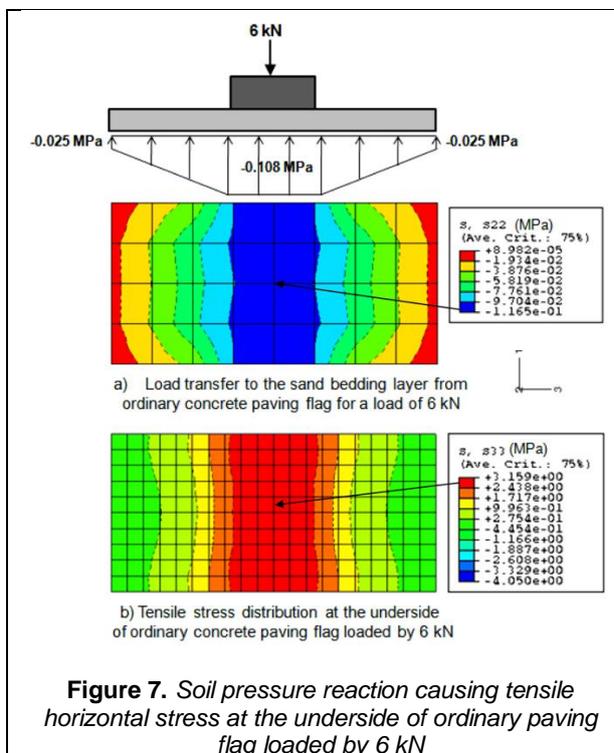**Table 2.** *Size and number of elements*

Part (dimension, mm)	Size of element (mm)	Number of elements
Sub-base (800x800x250 mm)	100x100x50	320
Sand bedding (800x800x40 mm)	50x50x20	512
Square loading plate (100x100x50 mm)	10x10x10	500
Factory flag (200x400x30 mm)	20x20x10	600

3. Results and Discussions

3.1 Paving flag - Stress, Strain and Failure load

The FEA modelling confirmed that the bending moment causing failure for a paving flag was created by the soil pressure reaction, as shown in Figures 7 and 8, for an ordinary concrete paving flag and an UHPFRC paving flag respectively. Figures 7a and 8a show the compressive vertical stresses in the sand bedding layers. It is noted that these compressive vertical stresses were caused by the loads transferring through paving flags. These stresses are considered as the soil pressure reaction applying on the undersides of paving flags.

The FEA modelling results indicated that the soil pressure reaction at the underside of the paving flag reduced gradually from the centre to the ends, see figures 7a and 8a. This is more detailed than that was assumed in empirical design methods, i.e. uniform soil pressure reaction. These soil pressures caused the tensile stresses at the undersides of paving flags. The maximum tensile horizontal stress is in dark colour and the minimum one is in bright colour, see figure 8b. Under the load of 6 kN and 18 kN, the tensile failure stresses of the ordinary concrete flag and the UHPFRC flag at the central underside were approximately 3.16 MPa (see figure 7b) and 11.98 MPa (see figure 8b) respectively.

Figure 7. *Soil pressure reaction causing tensile horizontal stress at the underside of ordinary paving flag loaded by 6 kN*

Figure 8. *Soil pressure reaction causing tensile horizontal stress at the underside of UHPFRC paving flag loaded by 18 kN*
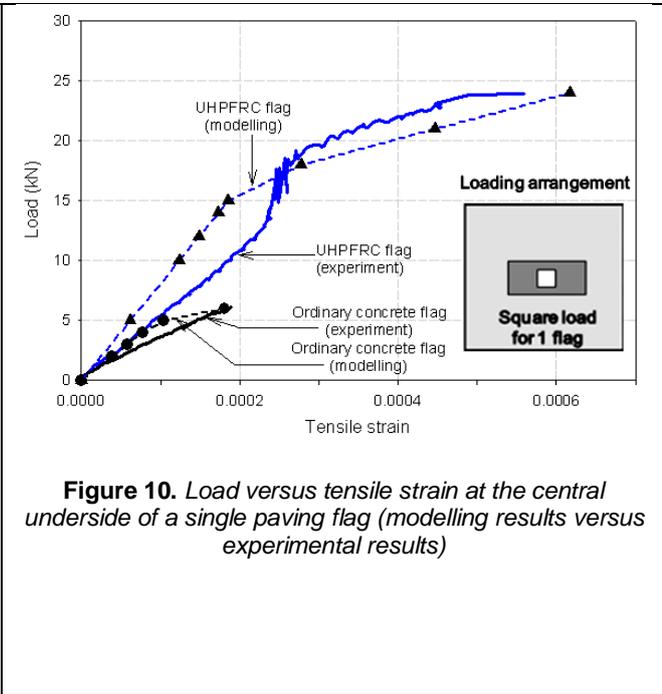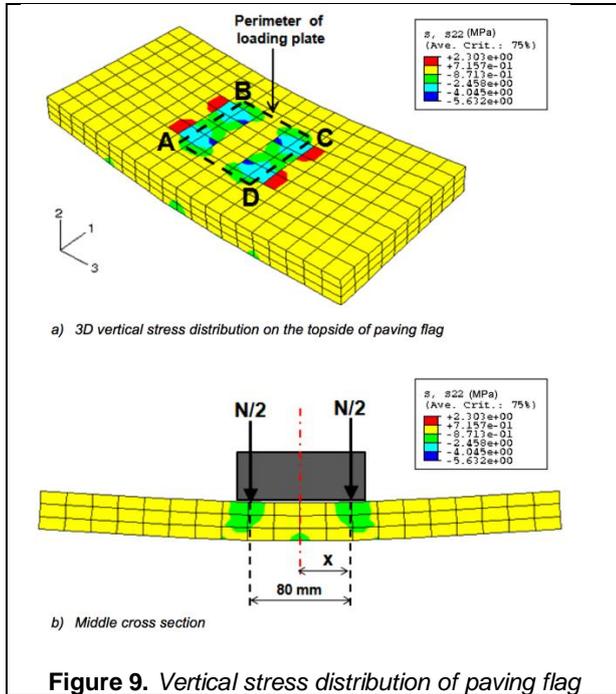
The mechanism of load transfer from the square loading plate to the flag can also be seen in the FEA models. The load almost all transferred within two regions near AB and CD edges as shown in figure 9, the load position (x – distance from central line to loading position) of 37 - 40 mm was reasonable. The FEA modelling results of the load versus tensile strain relationships showed a good agreement with the experimental results for both types of paving flags. These are detailed in figure 10. The failure

loads predicted by the FEA models were very close to the failure loads measured by experiments, i.e. 6 kN for the ordinary concrete paving flag and 19 kN for the UHPFRC paving flag. However, the failure

strains predicted by the FEA model appeared less than the experimental ones. This issue might result from the input material properties of the paving flags which were not identical to the experimental ones.


a) 3D vertical stress distribution on the topside of paving flag

b) Middle cross section

Figure 9. *Vertical stress distribution of paving flag*

Figure 10. *Load versus tensile strain at the central underside of a single paving flag (modelling results versus experimental results)*

3.2 Paving flag - Displacement

The different displacement behaviour of the UHPFRC paving flag and the ordinary concrete paving flag are shown in figures 11 and 12 respectively. The FEA modelling results agreed relatively well with the experimental results. Both of them indicated that the magnitudes of the displacements at different positions of the paving flag were unequal. The whole paving flag moved downwards and the displacement at the middle region (D2 and D3) under the square loading plate was larger than that at the two ends (D1 and D4).

For the pavement tested with an ordinary concrete flag, the FEA model only predicted the displacement of the paving flag until failure of the flag occurred, i.e. at an applied load of 6 kN. The model of an ordinary concrete paving flag was terminated at failure so the post-failure displacement of flag was not approachable as shown in figure 11.

For the pavement tested with a UHPFRC paving flag, the FEA model predicted the displacement of the flag until an applied load of 34 kN and the post-failure displacement, i.e. after the failure load of 18 kN, was also determined and is shown in figure 12.

Figure 11. *Load versus displacement - ordinary*

Figure 12. *Load versus displacement - UHPFRC*
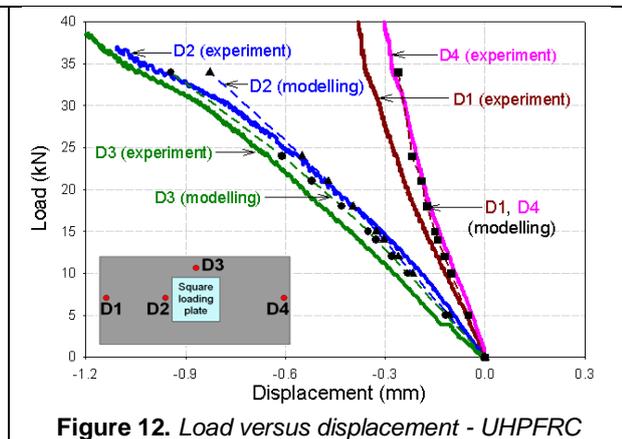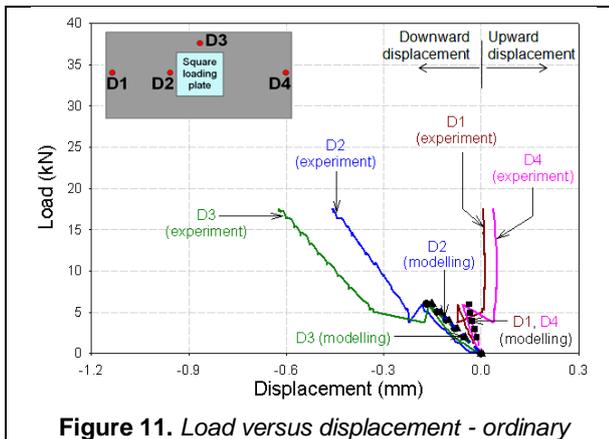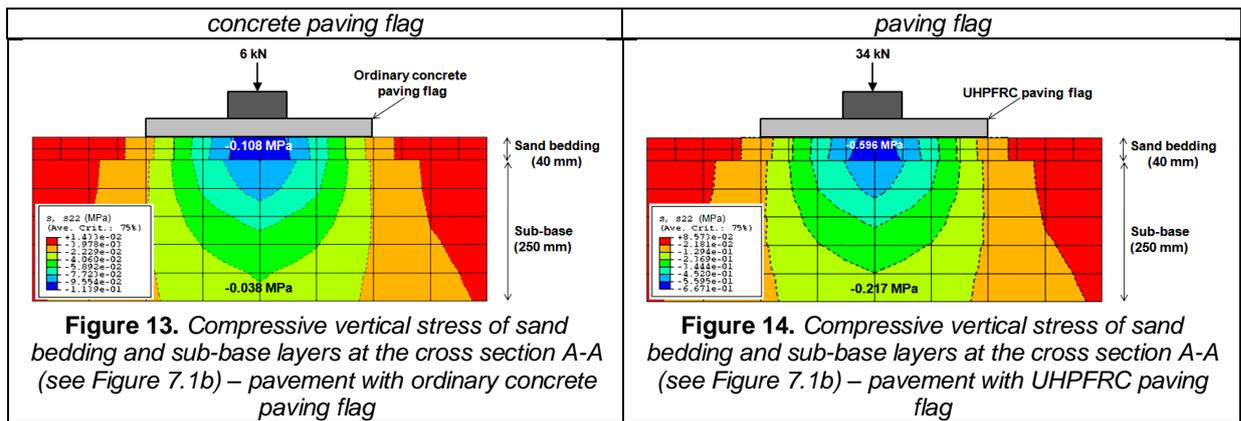
Figure 13. *Compressive vertical stress of sand bedding and sub-base layers at the cross section A-A (see Figure 7.1b) – pavement with ordinary concrete paving flag*

Figure 14. *Compressive vertical stress of sand bedding and sub-base layers at the cross section A-A (see Figure 7.1b) – pavement with UHPFRC paving flag*
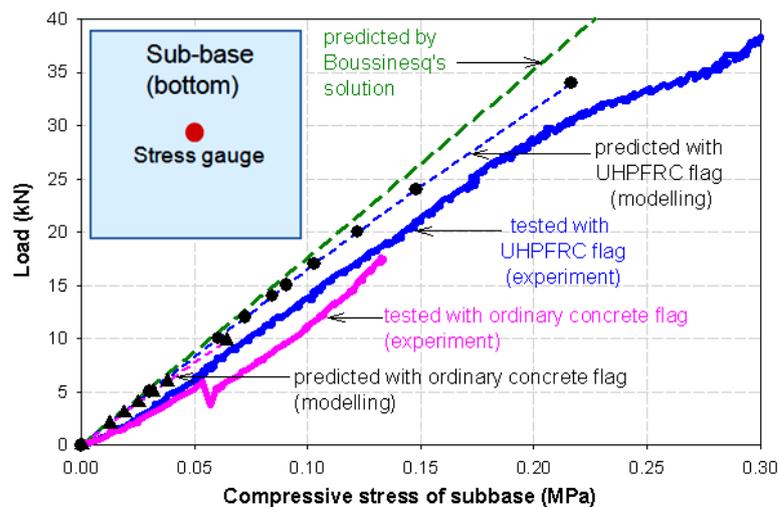
Figure 15. *Load versus compressive stress at the central bottom of sub-base layer*

3.3 Structural behaviour of sand bedding and sub - base layers

The behaviour of the sand bedding and sub-base layers in this model showed that they had met the main role of typical support layers, that is assisting in reducing the vertical stress transmitted from the load applied to the subgrade (under the sub-base), see figures 13, 14 and 15. The pressure was reduced by a factor of approximately 15 at the bottom of the sub-base in this case. In the case of an ordinary concrete paving flag, when a vertical load of 6 kN was applied, i.e. 0.6 MPa pressure, the compressive vertical stress at the central top of the sand bedding and at the central bottom of the sub-base were only 0.108 MPa and 0.038 MPa respectively. Besides, the compressive vertical stresses in the pavement using a UHPFRC paving flag were only 0.596 MPa for the central top of sand bedding and 0.217 MPa for the central bottom of sub-base layer when a load of 34 kN, i.e. 3.4 MPa pressure, was applied. The modelling results of compressive stress of the sub-base layer agreed relatively well with the experimental and theoretical results, as shown in figure 15.

In the FEA modelling of the pavement with an ordinary concrete flag, the compressive stress of the sub-base layer could not reduce at the load of 6 kN when the paving flag was broken, as occurred in the experiment, because the modelling material used for the sub-base layer was elastic (as assumed in the soil mechanics theory).

4. Conclusions

FEA modelling for a single paving flag loaded centrally showed that the predicted failure loads of the ordinary concrete paving flag and the UHPFRC paving flag were very close to the experimental results, i.e. 6 kN for the ordinary concrete paving flag and 19 kN for the UHPFRC paving flag. The load versus tensile strain relationships and load versus displacement relationships generally agreed with the experimental behaviours. Furthermore, FEA models would predict the failure loads of flags that could not be obtained by the experiments.

FEA modelling also showed clearly the mechanism of load transfer through paving flags to the sand bedding and sub-base layers. Therefore, the reasons for failure of paving flags are clarified, e.g. the movements of paving flags and the distributions of sand reaction pressure on the underside of paving flags.

FEA modelling of a pavement section with a single paving flag loaded centrally was implemented successfully. The model could be used to perform the changes in structural behaviour when the thickness and other properties of the flag, the sand bedding and the sub-base layer are varied. This modelling approach helps to reduce the number of experiments. Therefore, the FEA modelling results efficiently contribute to the practical guidelines for structural design of flag pavements.

REFERENCES

[1] Fagan, M. J. (1997), Finite Element Analysis: Theory and Practice. *pp. 315.*

[2] Mottram, J. T., Shaw, C. T. (1996), Using Finite Elements in Mechanical Design. *McGraw-Hill International (UK) Ltd. p. 276.*

[3] Bull, J. W. and Al-Khalid, H. (1987), An Analytical Solution to The Design of Footway Paving Flags. *Computers and Geotechnics, 4, pp. 85-96.*

[4] Bull, J. W. (1988), The design of footway paving flags. *Highways (Croydon, England), 56(1936), pp. 44-45.*

[5] Liu, W. and Fwa, T. F.(2007), Nine-slab model for jointed concrete pavements. *International Journal of Pavement Engineering, 8(4), pp. 277-306.*

[6] Ioannides, A. M., Peng, J., Swindler, J. R. (2006), ABAQUS model for PPC slab cracking. *The International Journal of Pavement Engineering, Vol. 7(No. 4), pp. 311-322.*

[7] Falkner, H., Huang, Z., and Teutsch, M. (1995), Comparative study of plain and steel fiber reinforced concrete ground slabs. *Concrete International, 17(1), pp. 45-51.*

[8] Kim, M. and Tutumluer, E. (2006), Modeling nonlinear, stress-dependent pavement foundation behaviour using a general-purpose finite element program, Shanghai, China. *American Society of Civil Engineers, Reston, USA. pp. 29-36.*

[9] Al-Qadi, I. L. and Elseifi, M. A. (2006), Mechanism and modelling of transverse cracking development in continuously reinforced concrete pavement. *International Journal of Pavement Engineering, 7(4), pp. 341-349.*

[10] Cousins, T., Wollmann, C. R., and Sotelino, E. (2008), UHPC Deck Panels for Rapid Bridge Construction and Long Term Durability. *In The Second International Symposium on Ultra High Performance Concrete, Kassel, Germany. Kassel University Press. pp. 699-705.*

[11] Tanaka, Y., et al. (2008), Technical Development of a Long Span Monorail Girder Applying Ultra High Strength Fibre Reinforced Concrete. *In The Second International Symposium on Ultra High Performance Concrete, Kassel, Germany. Kassel University Press. pp. 803-811.*

[12] ABAQUS (2002), ABAQUS/Standard - User's Manual. *Hibbitt, Karlsson & Sorensen Inc., USA.*

[13] Hillerborg, A., Modéer, M., Petersson, P. -E. (1976), Analysis of crack formation and crack growth in concrete by means of fracture mechanics and finite elements. *Cement and Concrete Research, 6(6), pp. 773-781.*

[14] Rots, J.G. (1991), Computational modelling of concrete fracture. *Delft University of Technology, Netpherlands. p. 141.*

[15] Guzina, B. B., et al. (1995), Failure predictions of smeared-crack formulations. *Journal of Engineering Mechanics, 121(1), pp. 150-161.*

[16] Zhaoxia, L. and Mroz Z. (1994), A Viscoplastic Model Combined Smedamage and Smeared Crack for Softening of Concrete. *ACTA Mechanica Solida Sinica, 7(2), pp. 125-136.*

[17] ABAQUS (2002), ABAQUS Theory Manual. *Hibbitt, Karlsson & Sorensen Inc., USA.*

[18] Acker, P. and Behloul, M. (2004), Ductal Technology: A Large Spectrum of Properties, A Wide Range of Applications. *In Proceedings of Ultra High Performance Concrete, September 13-15, Kassel, Germany. pp. 13-23.*

[19] Neville, A. M.(1995), Properties of Concrete. *Addison Wesley Longman Limited. p. 844.*

[20] Bangash, M. Y. H. (2001), Manual of Numerical Methods in Concrete. *Thomas Telford. p. 918.*